

Abstract

Standard climate projections represent future volcanic eruptions by a constant forcing inferred from 1850-2014 volcanic forcing. Using the latest ice-core and satellite records to design stochastic eruption scenarios, we show that there is a 95% probability that explosive eruptions could emit more sulfur dioxide (SO₂) into the stratosphere over 2015-2100 than current standard climate projections (i.e., ScenarioMIP). Our simulations using the UK Earth System Model with interactive stratospheric aerosols show that for a median future eruption scenario, the 2015-2100 average global-mean stratospheric aerosol optical depth (SAOD) is double that used in ScenarioMIP, with small-magnitude eruptions (< 3 Tg of SO₂) contributing 50% to SAOD perturbations. We show that volcanic effects on large-scale climate indicators, including global surface temperature, sea level and sea ice extent, are underestimated in ScenarioMIP because current climate projections do not fully account for the recurrent frequency of volcanic eruptions of different magnitudes.

Plain Language Summary

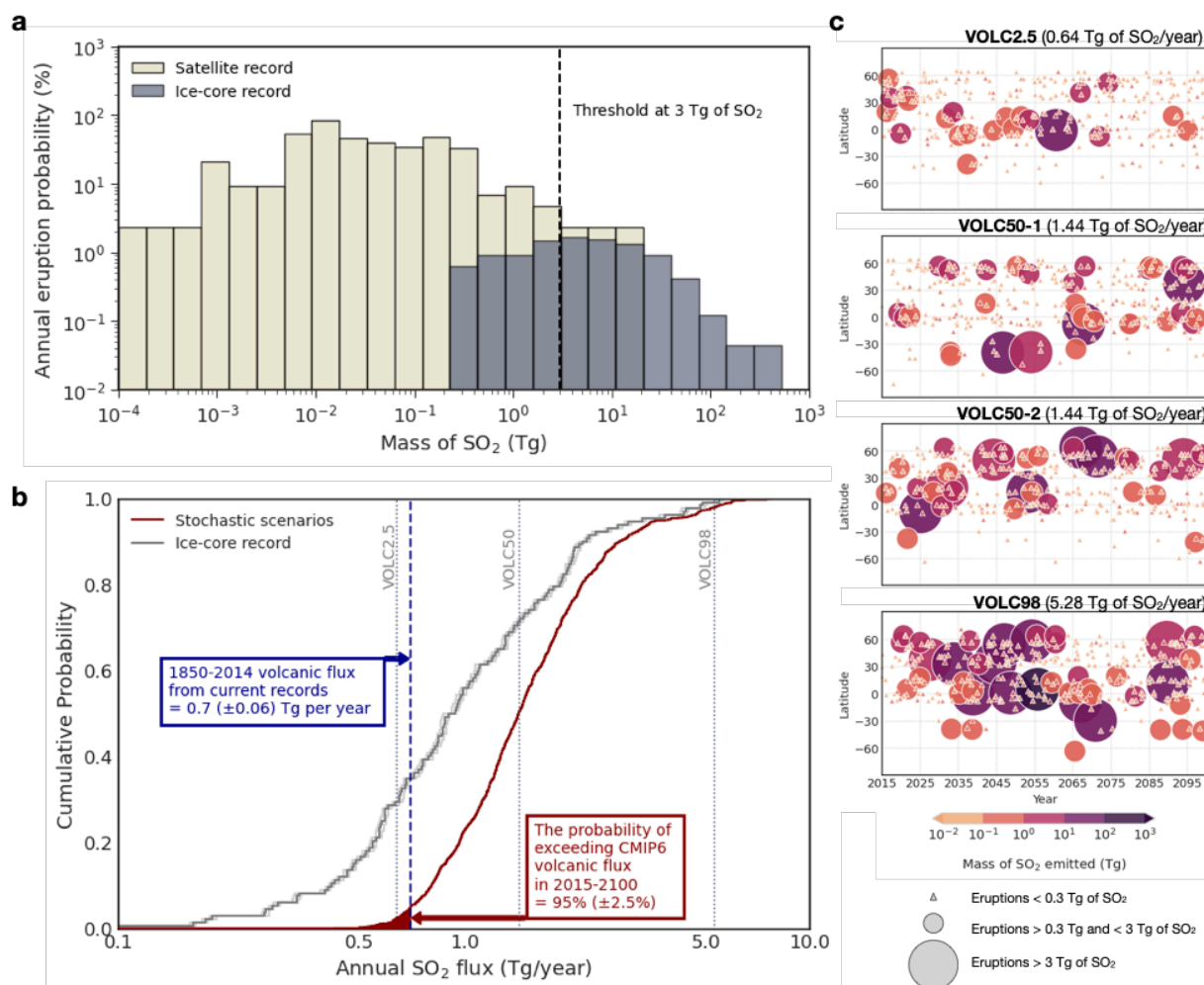
Climate projections are the simulations of Earth's climate in the future using complex climate models. Standard climate projections, as in Intergovernmental Panel on Climate Change Sixth Assessment Report, assume that explosive volcanic activity over 2015-2100 are of the same level as the 1850-2014 period. Using the latest ice-core and satellite records, we find that explosive eruptions could emit more sulfur dioxide into the upper atmosphere for the period of 2015-2100 than standard climate projections. Our climate model simulations show that the impacts of volcanic eruptions on climate, including global surface temperature, sea level and sea ice extent, are underestimated because current climate projections do not fully account for the recurrent frequency of volcanic eruptions. We also find that small-magnitude eruptions occur frequently and can contribute a significant effect on future climate.

1. Introduction

Large explosive volcanic eruptions can inject sulfur dioxide (SO₂) forming volcanic sulfate aerosols in the stratosphere that scatter incoming solar radiation, resulting in negative radiative forcing and global surface cooling for 1-3 years (McCormick et al., 1995). Stratospheric volcanic sulfate aerosols also heat the stratosphere by absorbing infrared and near-infrared radiation, which can further induce complex climate responses on seasonal to multi-decadal timescales (see Marshall et al. (2022) for a review).

As we cannot predict future volcanic eruptions, a constant volcanic forcing is commonly used in climate projections, e.g., as done in Phase 6 of the Coupled Model Intercomparison Project (CMIP6; Eyring et al., 2016), which informs the Intergovernmental Panel on Climate Change (IPCC) Sixth Assessment Report. In the CMIP6 Scenario MIP (ScenarioMIP; O'Neill et al., 2016), the constant volcanic forcing is inferred from the time average of the reconstructed 1850-2014 volcanic forcing. This approach does not account for how the sporadic occurrence of volcanic eruptions may affect the climate as opposed to a time-averaged forcing. In addition, volcanic injections into the stratosphere during the Holocene (past 11,500 years; Sigl et al., 2022) can vary

76 by as much as a factor of 25 on centennial timescales. The corresponding uncertainty on future
 77 volcanic forcing is currently unaccounted for in most climate projections. A handful of studies
 78 have attempted to quantify the role of volcanic forcing uncertainty in climate projections (Ammann
 79 and Naveau, 2010; Bethke et al., 2017; Dogar et al., 2020). Bethke et al. (2017) estimated the
 80 volcanic forcing of 60 different future eruption scenarios from 2015 to 2100 by resampling ice-
 81 core sulfate deposition records going back 2,500 years (Sigl et al., 2015). Up-to-date ice-core and
 82 satellite volcanic sulfur emission datasets enable us to account for the occurrence of (i) eruptions
 83 larger in magnitude than those that occurred between 1850 and 2014, which injected as much as
 84 300 Tg of SO₂ into the atmosphere, and (ii) small-magnitude eruptions below the detection
 85 threshold of ice-core datasets (Figure 1a), which can contribute a significant fraction to
 86 stratospheric aerosol optical depth (SAOD) (Santer et al., 2014; Schmidt et al., 2018).
 87



88 **Figure 1.** (a) Annual eruption probability based on ice-core (Sigl et al., 2022) and satellite (Carn
 89 et al., 2022) datasets. (b) Empirical cumulative probability density function of the SO₂ mass
 90 distribution of the 1000-member stochastic scenarios and the Holvol ice-core dataset (with 95%
 91 bootstrap confidence bounds, in light grey). We estimate the probability of exceeding CMIP6
 92 volcanic flux using the 1850-2014 flux from current volcanic SO₂ emission records (Neely and
 93 Schmidt, 2016; Sigl et al., 2022; Carn, 2022). (c) Eruption time series of VOLC2.5, VOLC50-1,
 94 VOLC50-2, and VOLC98 with annual volcanic SO₂ flux of each scenario in brackets.
 95

96
97
98
99
100
101
102
103
104
105
106
107
108
109

In addition, whether they apply a constant volcanic forcing (e.g., CMIP6 ScenarioMIP) or use stochastic eruption scenarios (Bethke et al., 2017), existing climate projections use prescribed volcanic aerosol optical properties derived from simplified volcanic aerosol models. Climate models with interactive stratospheric aerosols (Timmreck et al., 2018) showed a better agreement between the simulated surface temperature responses and tree-ring surface temperature reconstructions for the 1257 Mount Samalas and 1815 Mount Tambora eruptions (Stoffel et al., 2015) and the 1783-1784 Laki eruption (Pausata et al., 2015; Zambri et al., 2019). Furthermore, the prescribed aerosol approach cannot account for the impacts of global warming on the life cycle of volcanic sulfate aerosols (Aubry et al., 2021), including the impact of changing atmospheric stratification on volcanic plume height (Aubry et al., 2019). Such climate-volcano feedbacks might amplify the peak global-mean radiative forcing associated with large-magnitude tropical eruptions by 30% (Aubry et al., 2021).

110
111
112
113
114
115
116
117

Our study aims to improve our understanding of future volcanic impacts on climate. To this end, we perform model simulations from 2015 to 2100 with two innovations: (i) a stochastic resampling approach using the latest ice-core and satellite datasets to generate improved future volcanic eruption scenarios; and (ii) a plume-aerosol-chemistry-climate modeling framework (named UKESM-VPLUME), which combines a volcanic plume model and an Earth System Model with interactive stratospheric aerosols to simulate volcanic climate effects while accounting for climatic controls on plume-rise height.

118
119

2. Methodology

120
121

2.1 Stochastic future eruption scenarios

122
123
124
125
126
127
128
129
130
131
132
133
134
135
136
137

We generate 1000 stochastic future eruption scenarios for 2015 to 2100 by resampling SO_2 mass from volcanic emission inventories from a bipolar ice-core array covering the past 11,500 years (Holvol; Sigl et al., 2022) and a multi-satellite record from 1979 to 2021 (Carn et al., 2016; Carn, 2022) (Figure 1a and S1). Before resampling, we filter out: i) effusive eruptions; ii) in the satellite record, eruptions with eruptive plume heights more than 3 km below the thermal tropopause (obtained from NCEP/NCAR Reanalysis 1; Kalnay et al., 1996); we assume that aerosol lofting could result in stratospheric injections for tropospheric plumes less than 3 km below the tropopause. By examining the eruption frequency-magnitude (i.e., in this study, SO_2 mass) distribution of both ice-core and satellite records (Figure 1a), we identify 3 Tg of SO_2 as a threshold: i) below which ice-core records underestimate eruption frequency due to under-recording; and ii) above which the short duration of the satellite record precludes it from capturing the true frequency of eruptions with higher magnitude. Accordingly, we use a 3 Tg of SO_2 threshold to define “small-magnitude” and “large-magnitude” eruptions. We resample small-magnitude eruptions from the satellite record only, and large-magnitude ones from the combined ice-core and satellite record. Details of the resampling of the erupting volcano, SO_2 mass, and mass eruption rate are discussed in the Supplementary Information.

138
139
140
141

2.2 UKESM-VPLUME

142 Atmospheric stratification, wind and humidity affect volcanic plume dynamics and SO₂
143 injection height (e.g., Mastin, 2014), but SO₂ height is commonly prescribed in modelling studies
144 of volcanic forcing (e.g., Timmreck et al., 2018). To account for meteorological controls on plume
145 dynamics, we have developed UKESM-VPLUME, which couples the UK Earth System Model
146 (UKESM; Mulcahy et al., 2023) with Plumeria (1-D eruptive plume model; Mastin, 2007, 2014)
147 (details in Supplementary Information). We use version 1.1 of UKESM with fully-coupled
148 atmosphere-land-ocean and interactive stratospheric aerosols. In brief, for each time step of the
149 UKESM atmospheric model during an eruption, UKESM-VPLUME interactively passes the
150 atmospheric conditions simulated at the eruption location to Plumeria. Plumeria then computes the
151 neutral buoyancy height of the volcanic plume based on atmospheric conditions and the mass
152 eruption rate generated for each eruption in the stochastic scenarios. Volcanic SO₂ is injected into
153 UKESM at the neutral buoyancy height calculated in Plumeria using a gaussian profile with a
154 width of 10% of the plume height (consistent with large-eddy simulations of volcanic plumes,
155 Aubry et al., 2019). This approach ensures that plume heights of volcanic eruptions are consistent
156 with the meteorological conditions simulated by UKESM.

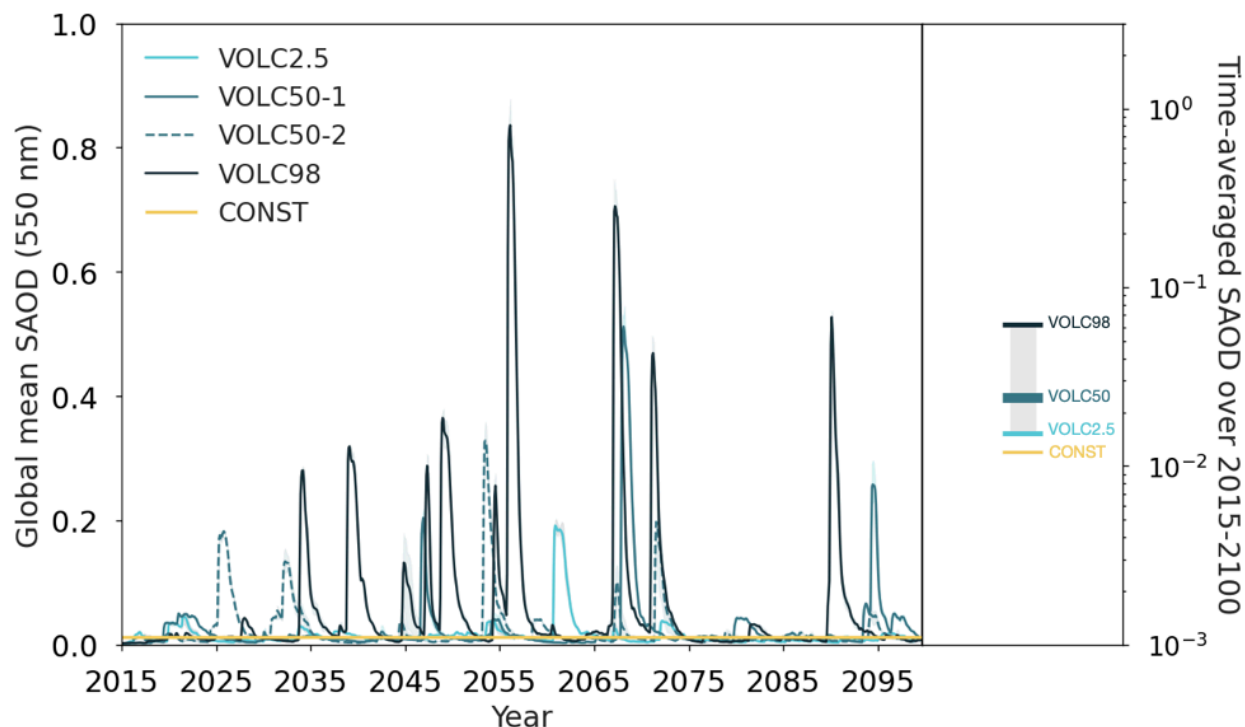
157 2.3 Experimental design

160 We perform simulations using the UKESM-VPLUME framework for four stochastic future
161 eruption scenarios at the 2.5th, 50.0th, 50.5th and 98.0th percentiles (termed VOLC2.5, VOLC50-1,
162 VOLC50-2, VOLC98) of the distribution of the 2015-2100 average SO₂ flux across the 1000 future
163 eruption scenarios (Figure 1b). We choose scenarios close (within 0.5 percentile) to the 2.5th, 50th
164 and 97.5th to sample the median and 95% confidence interval of the future volcanic stratospheric
165 SO₂ injections. To test future climate trajectory sensitivity to the temporal and spatial distribution
166 of eruptions, we run two scenarios near the 50th percentile. For instance, VOLC50-2 has more
167 large-magnitude eruptions than VOLC50-1 in the early 21st century (Figure 1c). We also
168 performed the VOLC50 runs with small-magnitude eruptions only (VOLC50-1S and VOLC50-
169 2S) to isolate their contribution to the overall climate effects caused by eruptions of all magnitudes.
170 We compare the results from VOLC runs with runs without volcanic eruptions (NOVOLC) and
171 with CMIP6 ScenarioMIP constant volcanic forcing (CONST). We perform all simulations from
172 2015 to 2100 under a high-end future emission scenario (SSP3-7.0 in ScenarioMIP) running three
173 ensemble members for each scenario.

174 3. Results

176 Figure 2 shows the global monthly-mean SAOD at 550 nm and the time-averaged values
177 over 2015-2100. The time-averaged ensemble-mean SAOD ranges from 0.015 ± 0.0004
178 (VOLC2.5) to 0.062 ± 0.0018 (VOLC98), with an average value of 0.024 ± 0.0012 for the two
179 median future eruption scenarios (VOLC50), while the SAOD in CONST, which followed the
180 ScenarioMIP design, is 0.012 ± 0.0018 (one standard deviation uncertainty). Small-magnitude
181 eruptions contribute 0.010 to 0.013 ± 0.0002 to the time-averaged SAOD in the VOLC50
182 scenarios, i.e., about 50% of the total SAOD. Comparing VOLC2.5 to CONST and assuming that
183 the rank for the 2015-2100-year mean volcanic SO₂ flux and SAOD are the same, it is thus very
184 likely (i.e., > 90% probability following IPCC guidance note; Mastrandrea et al., 2010) that the
185 actual global 2015-2100 mean SAOD will be higher than that prescribed in ScenarioMIP, with the
186 median (VOLC50) SAOD value being double that used in ScenarioMIP. The result is consistent

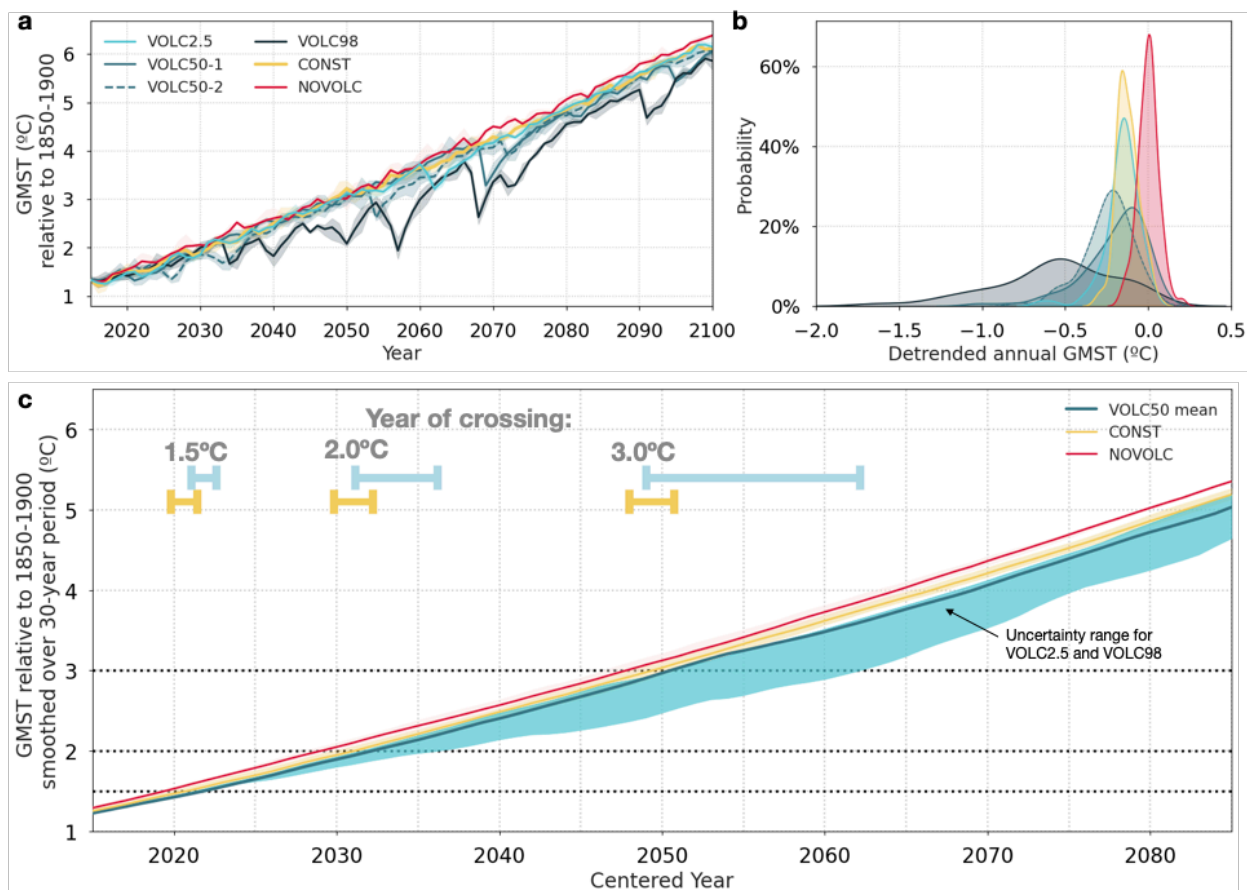
187 with Figure 1, given that the 1850-2014 time-averaged SO_2 flux used to define the ScenarioMIP
 188 volcanic forcing is close to the 2.5th percentile of the future volcanic SO_2 flux distribution. Beyond
 189 the time-averaged SAOD value, owing to the sporadic nature of volcanic eruptions, the global
 190 monthly-mean SAOD values in VOLC scenarios can be up to a factor of 60 greater than that in
 191 ScenarioMIP (Figures 2 and S2).



192 **Figure 2.** (Left) Global monthly-mean SAOD at 550 nm. The lines show the ensemble mean and
 193 the shading shows the spread of the maximum and minimum ensemble members. (Right) The
 194 corresponding time-averaged SAOD over 2015-2100 (in log scale).
 195

196 Figure 3a shows the global annual-mean surface air temperature at 1.5 m (GMST) relative
 197 to the 1850-1900 period. Large-magnitude volcanic eruptions lead to a short-term drop in the
 198 annual-mean GMST for at least 1 year and up to 6 to 7 years for the largest eruptions. In the
 199 VOLC98 scenario where clusters of large-magnitude eruptions occur, they can induce multi-
 200 decadal global cooling. The 2015-2100 time-averaged GMST relative to detrended NOVOLC
 201 ensemble mean (Figure 3b) ranges between -0.16 °C (VOLC2.5) and -0.56 °C (VOLC98), with
 202 CONST lying outside this range at -0.12 °C. Volcanic cooling for median eruption scenarios
 203 (VOLC50-1 and VOLC50-2) is 0.20 to 0.24 °C, double that of CONST, and 0.09 to 0.10 °C of
 204 cooling is attributable to small-magnitude eruptions (Table S1).

205

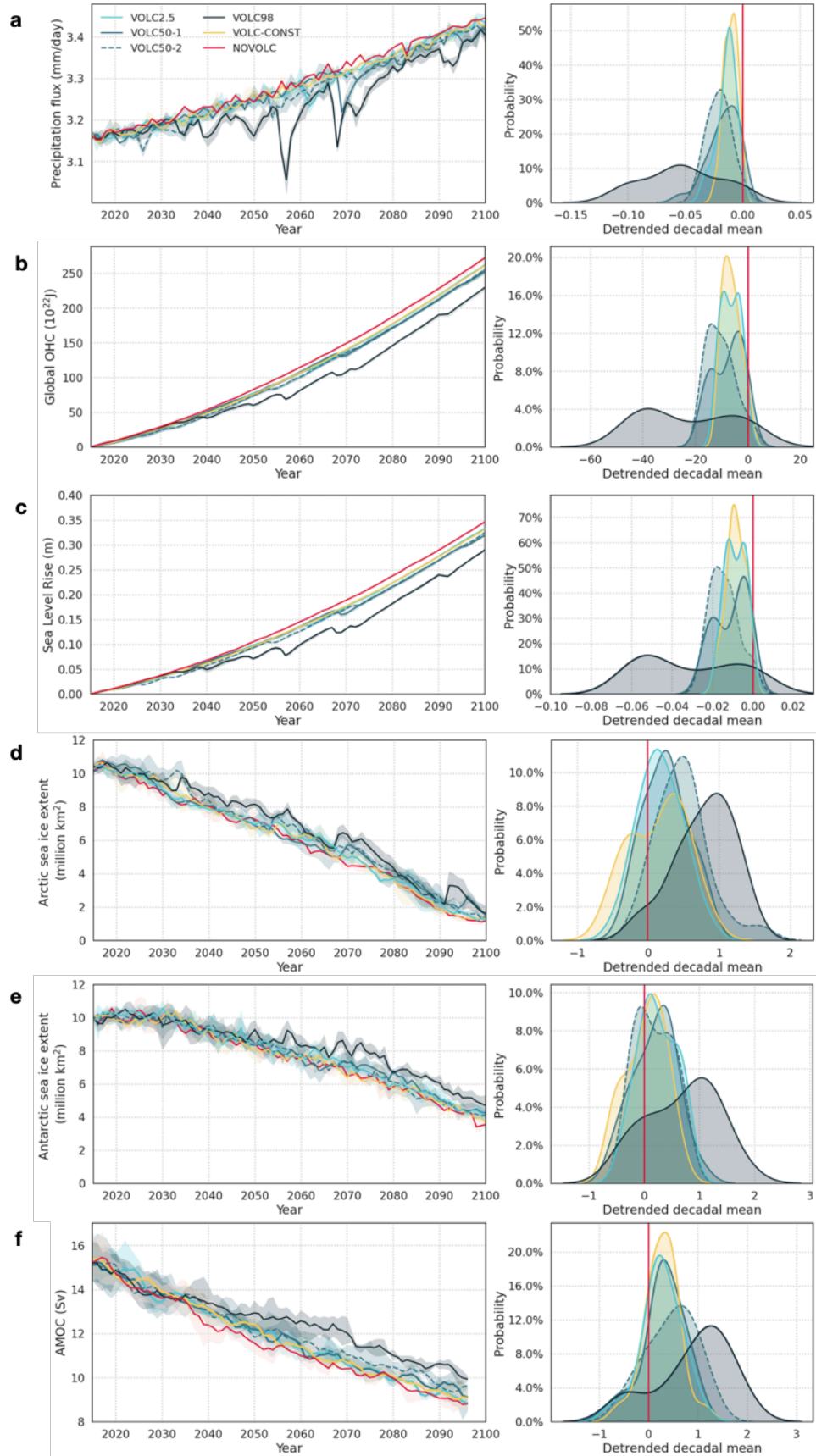


206
 207 **Figure 3.** (a) Annual-mean GMST relative to 1850-1900. The lines show the ensemble mean and
 208 the shading shows the spread of the maximum and minimum ensemble members. (b) Probability
 209 density function of the annual-mean GMST relative to detrended NOVOLC ensemble mean (see
 210 Supplementary Information). (c) 30-year moving mean GMST with years of crossing 1.5 °C, 2
 211 °C, and 3 °C for VOLC and CONST runs.
 212

213 The IPCC defines global warming as an increase, relative to 1850-1900, in the global mean
 214 surface air and sea surface temperatures over a period of 30 years (IPCC, 2021). Using this
 215 definition, we examine the year of crossing of 1.5 °C, 2 °C, and 3 °C warming thresholds for VOLC
 216 and CONST runs (Figure 3c). Volcanic eruptions delay the time of crossing 1.5 °C by about 1.6 to
 217 3.2 years when compared to NOVOLC (Table S2), consistent with Bethke et al. (2017). Compared
 218 to CONST, times of temperature threshold crossings are significantly delayed by 1.8 to 2.5 years
 219 in VOLC50-2, but unaffected in VOLC50-1. This highlights the sensitivity of the time of crossing
 220 to the temporal distribution of large-magnitude eruptions. The occurrence of volcanic clusters in
 221 VOLC98 causes an extended cooling period between 2034 to 2060 (Figure 3a) which delays the
 222 crossing of 2 °C and 3 °C by 7 and 14 years, respectively.

223 In Figure 4, we examine volcanic effects on large-scale climate indicators other than
 224 GMST. The 2015-2100 time-averaged global annual-mean precipitation fluxes in all VOLC runs
 225 show a greater reduction than CONST, with a range between -0.014 mm/day (VOLC2.5) to -0.052
 226 mm/day (VOLC98), and -0.010 mm/day for CONST (Figure 4a). In VOLC50 scenarios, the global

227 annual-mean precipitation flux is reduced by 0.019 mm/day with small-magnitude eruptions alone
228 contributing between 0.008 and 0.009 mm/day, comparable to the effects of the volcanic forcing
229 implemented in ScenarioMIP. It is thus very likely that the reduction of global mean precipitation
230 due to volcanic effects is underestimated in ScenarioMIP.



232
233
234
235
236
237
238
239
240

Figure 4. (Left) Annual mean time series of selected large-scale climate indicators. The line shows the ensemble mean and the shading shows the spread of the maximum and minimum ensemble members. (Right) The corresponding decadal-mean probability density function relative to the detrended NOVOLC ensemble mean, with the red vertical line showing the mean of NOVOLC. **(a)** global precipitation flux (in mm/day), **(b)** global ocean heat content (in 10^{22} J), **(c)** global thermosteric sea level rise (in m), **(d and e)** Arctic and Antarctic sea ice extent (in million km^2), defined as the area with $>15\%$ sea ice, **(f)** 5-year moving mean AMOC at 26°N (in Sv).

241
242
243
244
245
246
247
248

Volcanic-induced surface cooling penetrates into the deep ocean layer and decreases the global ocean heat content (Figures 4b and S3), which in turn leads to less thermal expansion in seawater and a reduction in thermosteric sea level (Figure 4c). Volcanic forcing in VOLC50 reduces global ocean heat content and thermosteric sea level by 6% to 7% compared to NOVOLC by 2100, whereby about half is attributed to small-magnitude eruptions (Figure S3). Although volcanic forcing can cause considerable impacts on large-scale ocean metrics, it does not offset the anthropogenic-induced ocean warming trends even for the upper-end volcanic emission scenario VOLC98 (Figures 4b, 4c and 4f).

249
250
251
252
253
254
255

Depending on the eruption magnitude and location, the Arctic and Antarctic sea ice extents show an immediate increase for 1-2 years after large-magnitude eruptions (Figures 4d and 4e). The time-averaged global sea ice extent in VOLC runs over 2015 to 2100 increases by 0.43 million km^2 (VOLC2.5) to 1.53 million km^2 (VOLC98) as compared to 0.20 million km^2 for CONST. Comparing VOLC2.5 to CONST suggests that for similar time-averaged SAOD, the use of a constant forcing instead of a stochastic eruption distribution halves the magnitude of the sea ice response.

256
257
258
259
260
261
262
263
264
265
266
267
268

The time-averaged Atlantic Meridional Overturning Circulation (AMOC) at 26°N over 2015 to 2100 is strengthened by between 0.26 Sv (VOLC2.5) and 0.93 Sv (VOLC98) as compared to NOVOLC, with all VOLC scenarios exhibiting an increased decadal mean AMOC strength (Figure 4f). The stronger AMOC responses in VOLC runs are consistent with reduced precipitation over the Northern Hemisphere, which increases salinity and enhances deep-water formation (Pausata et al., 2015). Small-magnitude eruptions alone can increase the time-averaged AMOC strength by 0.36-0.38 Sv (VOLC50-1S and VOLC50-2S), which is greater than CONST at 0.28 Sv, and contribute to over 77% of the AMOC response in the median future scenarios (Table S1). One of the median future scenarios (VOLC50-1) has a weaker time-averaged AMOC than the same run with small-magnitude eruptions only (VOLC50-1S) due to an extended period of weakened AMOC after the occurrence of large-magnitude eruptions (Figure S4), suggesting AMOC may have different responses towards different latitudinal and SO_2 distributions of large-magnitude eruptions.

269
270

4. Discussion

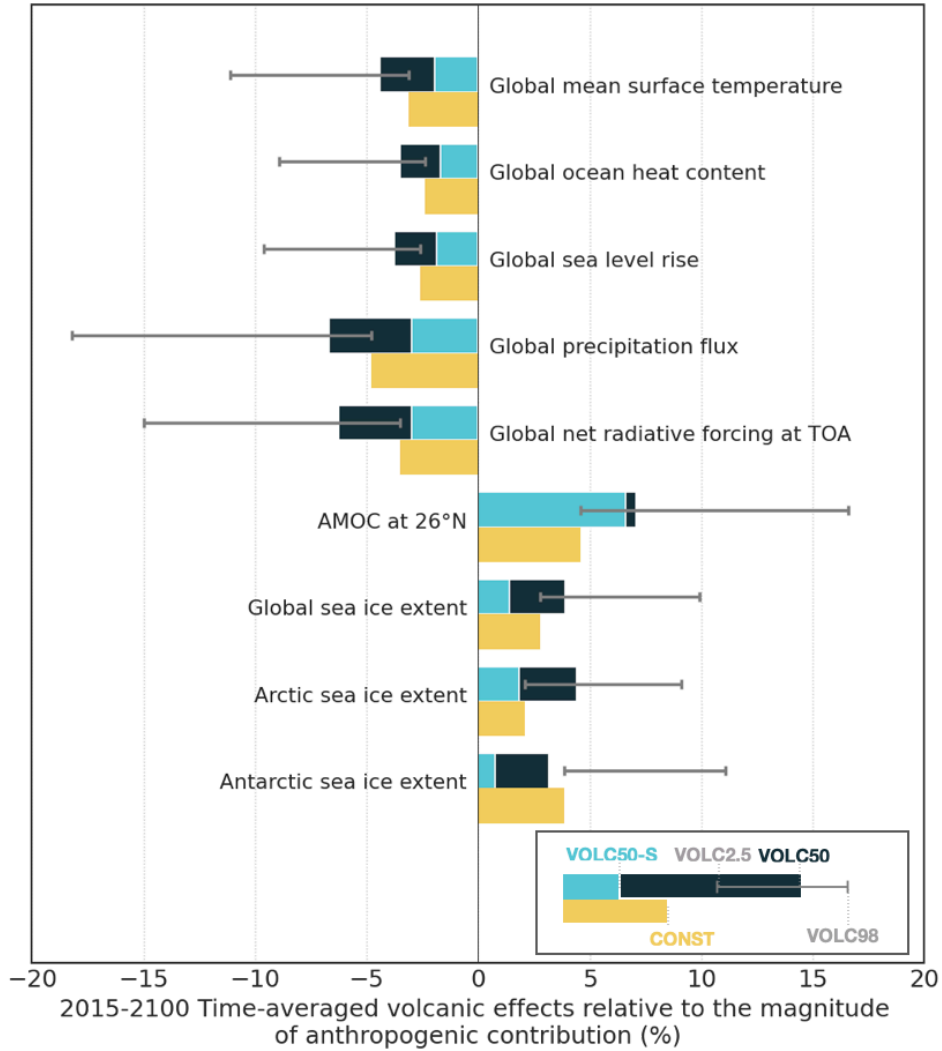
271
272
273
274

Small-magnitude eruptions ($< 3 \text{ Tg}$ of SO_2) contribute a considerable fraction (between 33% and 40%) of the total upper atmospheric volcanic SO_2 emissions in VOLC50, and in turn, are responsible for 30% to 50% of the volcanic impact on selected large-scale climate indicators and over 77% of the AMOC response (Figure 5 and Table S1). For future eruption scenarios with fewer

275 eruptions than VOLC50, the contribution from small-magnitude eruptions is expected to be even
276 greater because the total mass injected by small-magnitude eruptions is relatively similar across
277 all scenarios. Despite the importance of volcanic forcing from small-magnitude eruptions, they are
278 mostly unaccounted for in historical simulations before satellite measurements are available. In
279 the pre-satellite historical period (1850-1978), the Neely and Schmidt (2016) and Sigl et al. (2022)
280 volcanic SO₂ inventories have an average flux of 0.21 and 0.26 Tg of SO₂ per year from small-
281 magnitude eruptions, respectively. By comparison, the flux is 0.50 Tg of SO₂ per year over 1979-
282 2021 (Carn, 2022). This suggests a missing flux from small-magnitude eruptions of between 0.24
283 and 0.29 Tg of SO₂ per year in the pre-satellite historical period, which is the equivalent of
284 injections from about 1 to 2 Mount Pinatubo 1991 eruptions.
285

286 Our stochastic scenarios imply that CMIP6 ScenarioMIP very likely ($95 \pm 2.5\%$)
287 underestimates the 2015-2100 volcanic SO₂ flux from explosive eruptions and, in turn, forcing
288 (Figure 1b). Figure 1b shows the cumulative probability against the annual SO₂ flux obtained by
289 resampling ice-core record of volcanic SO₂ injection only (i.e., Holvol; Sigl et al. 2022) and both
290 ice-core and satellite (Carn, 2022) records as in our stochastic scenarios. CMIP6 ScenarioMIP uses
291 a constant volcanic forcing inferred from the 1850-2014 period during which the mean volcanic
292 SO₂ flux recorded in emission inventories was 0.7 ± 0.06 Tg per year. However, we find a 95%
293 confidence interval for the 2015-2100 mean volcanic SO₂ flux between 0.64 to 5.28 Tg per year
294 in our eruption scenarios (Figure 1b). Our stochastic approach, which represents better the
295 frequency-magnitude distribution of small-magnitude eruptions, results in a higher annual SO₂
296 flux than resampling from the ice-core record only (e.g., Bethke et al., 2017).
297

298 Our future volcanic eruption scenarios greatly enhance the variability of large-scale climate
299 indicators as compared to the ScenarioMIP forcing (Figure 5). Future volcanic emissions in our
300 scenarios cause a 3.5% (VOLC2.5) to 15.0% (VOLC98) decrease in the 2015-2100 time-averaged
301 global net radiative forcing at the top-of-the-atmosphere relative to the anthropogenic contribution
302 (Figures 5 and S5, see Supplementary Information). The time-averaged climate responses of our
303 selected climate indicators scale with the magnitude of volcanic forcing except for the Antarctic
304 sea ice extent and AMOC, which may depend on the latitudinal distribution of eruptions. We also
305 find that the magnitude of volcanic effects on climate indicators are comparable between CONST
306 and VOLC2.5, which is a scenario with only one Pinatubo-like eruption over 2015-2100. Our
307 results suggest that due to the low volcanic forcing used in ScenarioMIP, it is very likely (97.5%)
308 that ScenarioMIP underestimates the climate effects of the large-scale climate indicators examined
309 in this study.



310
 311 **Figure 5.** Bar chart showing the time-averaged volcanic effects on large-scale climate indicators
 312 relative to the magnitude of anthropogenic contribution over the period of 2015 to 2100, i.e.,
 313 VOLC50-S refers to average effects of the two VOLC50 runs with small-magnitude eruptions
 314 only.

315
 316 Our simulation results show that for the SSP3-7.0 scenario, volcanic forcing can offset
 317 2.1% to 18.2% of the anthropogenic effects to large-scale climate indicators depending on the
 318 future eruption scenarios (Figure 5). In a future scenario with low-end anthropogenic emission
 319 (SSP1-2.6), we would expect the relative effect between future volcanism and anthropogenic
 320 forcing to be much greater, e.g., by a factor of 3 for GMST since the 2015-2100 warming is 4.8 °C
 321 in SSP3-7.0 and 1.4 °C in SSP1-2.6. Our work highlights how the high level of uncertainty on
 322 volcanic forcing affects climate projections. For the same future eruption scenario, the volcanic
 323 effects on climate will also vary between SSP scenarios owing to climate-volcano feedbacks (e.g.,
 324 Hopcroft et al., 2017; Fasullo et al., 2018; Aubry et al., 2022), which need to be quantified.

325
 326
 327

328 **5. Conclusion**

329

330 We performed climate model simulations from 2015 to 2100 with stochastic future
331 eruption scenarios using UKESM-VPLUME (a plume-aerosol-chemistry-climate model
332 framework that accounts for climate-volcano feedbacks) to examine how the uncertainties on
333 volcanic forcing affect climate projections. Using the latest ice-core and satellite datasets, we show
334 that the 2015 to 2100 volcanic SO₂ flux from explosive eruptions has a 95% probability to exceed
335 the 1850-2014 flux, which was used to derive volcanic forcing in CMIP6 ScenarioMIP. Our
336 simulations suggest that the time-averaged SAOD in a median future scenario is 0.024 (95%
337 uncertainty: 0.015-0.062), which is double that in ScenarioMIP, and that ScenarioMIP very likely
338 underestimates the future volcanic effects on climate. Our study emphasizes the importance of the
339 climate effects of future volcanic eruptions relative to the anthropogenic contribution, which even
340 for an upper end anthropogenic forcing scenario (SSP3-7.0) can range between 2.1% to 18.2% for
341 large-scale climate indicators. We also highlight the climate-relevance of small-magnitude
342 eruptions, which are responsible for 30% to 50% of the volcanic effects on selected climate
343 indicators. Future climate projection studies could either use our stochastic eruption scenarios
344 generated using state-of-the-art volcanic emission inventories, or use a time-averaged constant
345 forcing that better represents long-term volcanic activity and accounts for small-magnitude
346 eruption contributions.

347

348 **Acknowledgements**

349 The authors declare no conflict of interests. We sincerely thank Robin Smith and Till Kuhlbrodt
350 for their suggestions in the analysis, and Larry Mastin who provided the latest version of Plumeria
351 model for developing UKESM-VPLUME framework. M.M. Chim is supported by the Croucher
352 Foundation and The Cambridge Commonwealth, European & International Trust through a
353 Croucher Cambridge International Scholarship. Jane Mulcahy and Jeremy Walton were supported
354 Met Office Hadley Centre Climate Programme, funded by BEIS.

355

356 **Data Availability Statement**

357 The data presented in this study are available in the University of Cambridge data repository:
358 <https://doi.org/10.17863/CAM.94912>. All data used for this study is with the license Creative
359 Commons Attribution 4.0 International (CC-BY-4.0).

References

- 360
361
362 Ammann, C. M., & Naveau, P. (2010). A statistical volcanic forcing scenario generator
363 for climate simulations. *Journal of Geophysical Research: Atmospheres*, *115*(D5).
364 <https://doi.org/10.1029/2009JD012550>
365
- 366 Archibald, A. T., O'Connor, F. M., Abraham, N. L., Archer-Nicholls, S., Chipperfield,
367 M. P., Dalvi, M., Folberth, G. A., Dennison, F., Dhomse, S. S., Griffiths, P. T., Hardacre,
368 C., Hewitt, A. J., Hill, R. S., Johnson, C. E., Keeble, J., Köhler, M. O., Morgenstern, O.,
369 Mulcahy, J. P., Ordóñez, C., ... Zeng, G. (2020). Description and evaluation of the
370 UKCA stratosphere–troposphere chemistry scheme (StratTrop vn 1.0) implemented in
371 UKESM1. *Geoscientific Model Development*, *13*(3), 1223–1266.
372 <https://doi.org/10.5194/gmd-13-1223-2020>
373
- 374 Aubry, T. J., & Jellinek, A. M. (2018). New insights on entrainment and condensation in
375 volcanic plumes: Constraints from independent observations of explosive eruptions and
376 implications for assessing their impacts. *Earth and Planetary Science Letters*, *490*, 132–
377 142. <https://doi.org/10.1016/j.epsl.2018.03.028>
378
- 379 Aubry, T. J., Cerminara, M., & Jellinek, A. M. (2019). Impacts of Climate Change on
380 Volcanic Stratospheric Injections: Comparison of 1-D and 3-D Plume Model Projections.
381 *Geophysical Research Letters*, *46*(17–18), 10609–10618.
382 <https://doi.org/10.1029/2019GL083975>
383
- 384 Aubry, T. J., Staunton-Sykes, J., Marshall, L. R., Haywood, J., Abraham, N. L., &
385 Schmidt, A. (2021). Climate change modulates the stratospheric volcanic sulfate aerosol
386 lifecycle and radiative forcing from tropical eruptions. *Nature Communications*, *12*(1),
387 4708. <https://doi.org/10.1038/s41467-021-24943-7>
388
- 389 Aubry, T. J., Farquharson, J. I., Rowell, C. R., Watt, S. F., Pinel, V., Beckett, F., Fasullo,
390 J., Hopcroft, P. O., Pyle, D. M., Schmidt, A., & Sykes, J. S. (2022). Impact of climate
391 change on volcanic processes: current understanding and future challenges. *Bulletin of*
392 *Volcanology*, *84*(6), 1–11. <https://doi.org/10.1007/s00445-022-01562-8>
393
- 394 Bethke, I., Outten, S., Otterå, O. H., Hawkins, E., Wagner, S., Sigl, M., & Thorne, P.
395 (2017). Potential volcanic impacts on future climate variability. *Nature Climate Change*,
396 *7*(11), 799–805. <https://doi.org/10.1038/nclimate3394>
397
- 398 Butchart, N. (2014). The Brewer-Dobson circulation. *Reviews of geophysics*, *52* (2),
399 157–184. <https://doi.org/10.1002/2013RG000448>
400
- 401 Carn, S. A., Clarisse, L., & Prata, A. J. (2016). Multi-decadal satellite measurements of
402 global volcanic degassing. *Journal of Volcanology and Geothermal Research*, *311*, 99–
403 134. <https://doi.org/10.1016/j.jvolgeores.2016.01.002>
404

- 405 Carn, S. (2022). *Multi-Satellite Volcanic Sulfur Dioxide L4 Long-Term Global Database*
406 *V4 (MSVOLSO2L4 4)* [Data set]. Goddard Earth Science Data and Information Services
407 Center (GES DISC). https://disc.gsfc.nasa.gov/datasets/MSVOLSO2L4_4/summary
408
- 409 Costa, A., Suzuki, Y. J., Cerminara, M., Devenish, B. J., Ongaro, T. E., Herzog, M., Van
410 Eaton, A. R., Denby, L., Bursik, M., Vitturi, M. d., et al. (2016). Results of the eruptive
411 column model inter-comparison study. *Journal of Volcanology and Geothermal*
412 *Research*, 326, 2–25. <https://doi.org/10.1016/j.jvolgeores.2016.01.017>
413
- 414 Devenish, B., & Cerminara, M. (2018). The transition from eruption column to umbrella
415 cloud. *Journal of Geophysical Research: Solid Earth*, 123(12), 10–418.
416 <https://doi.org/10.1029/2018JB015841>
417
- 418 Dhomse, S. S., Emmerson, K. M., Mann, G. W., Bellouin, N., Carslaw, K. S.,
419 Chipperfield, M. P., Hommel, R., Abraham, N. L., Telford, P., Braesicke, P., Dalvi, M.,
420 Johnson, C. E., O'Connor, F., Morgenstern, O., Pyle, J. A., Deshler, T., Zawodny, J. M.,
421 & Thomason, L. W. (2014). Aerosol microphysics simulations of the Mt. Pinatubo
422 eruption with the UM-UKCA composition-climate model. *Atmospheric Chemistry and*
423 *Physics*, 14(20), 11221–11246. <https://doi.org/10.5194/acp-14-11221-2014>
424
- 425 Dogar, M. M., Sato, T., & Liu, F. (2020). Ocean Sensitivity to Periodic and Constant
426 Volcanism. *Scientific Reports*, 10(1), 293. <https://doi.org/10.1038/s41598-019-57027-0>
427
- 428 Eyring, V., Bony, S., Meehl, G. A., Senior, C. A., Stevens, B., Stouffer, R. J., & Taylor,
429 K. E. (2016). Overview of the Coupled Model Intercomparison Project Phase 6 (CMIP6)
430 experimental design and organization. *Geoscientific Model Development*, 9(5), 1937–
431 1958. <https://doi.org/10.5194/gmd-9-1937-2016>
432
- 433 Fasullo, J. T., Tilmes, S., Richter, J. H., Kravitz, B., MacMartin, D. G., Mills, M. J., &
434 Simpson, I. R. (2018). Persistent polar ocean warming in a strategically geoengineered
435 climate. *Nature Geoscience*, 11(12), 910–914. [https://doi.org/10.1038/s41561-018-0249-](https://doi.org/10.1038/s41561-018-0249-7)
436 [7](https://doi.org/10.1038/s41561-018-0249-7)
437
- 438 Fero, J., Carey, S. N., & Merrill, J. T. (2009). Simulating the dispersal of tephra from the
439 1991 Pinatubo eruption: Implications for the formation of widespread ash layers. *Journal*
440 *of Volcanology and Geothermal Research*, 186(1-2), 120-131.
441 <https://doi.org/10.1016/j.jvolgeores.2009.03.011>
442
- 443 Gautier, E., Savarino, J., Hoek, J., Erbland, J., Caillon, N., Hattori, S., Yoshida, N.,
444 Albalat, E., Albarede, F., & Farquhar, J. (2019). 2600-years of stratospheric volcanism
445 through sulfate isotopes. *Nature Communications*, 10(1), 466.
446 <https://doi.org/10.1038/s41467-019-08357-0>
447
- 448 Global Volcanism Program (2022). *Volcanoes of the World* (v. 4.11.1; 29 Aug 2022).
449 [Database]. Distributed by Smithsonian Institution, compiled by Venzke, E.
450 <https://doi.org/10.5479/si.GVP.VOTW5-2022.5.0>

- 451
452 Guo, S., Bluth, G. J., Rose, W. I., Watson, I. M., & Prata, A. J. (2004). Re-evaluation of
453 SO₂ release of the 15 June 1991 Pinatubo eruption using ultraviolet and infrared satellite
454 sensors. *Geochemistry, Geophysics, Geosystems*, 5(4).
455 <https://doi.org/10.1029/2003GC000654>
456
- 457 Hersbach, H., Bell, B., Berrisford, P., Biavati, G., Horányi, A., Muñoz Sabater, J.,
458 Nicolas, J., Peubey, C., Radu, R., Rozum, I., Schepers, D., Simmons, A., Soci, C., Dee,
459 D., Thépaut, J.-N. (2019). *ERA5 monthly averaged data on pressure levels from 1979 to*
460 *present* [Data set]. Copernicus Climate Change Service (C3S) Climate Data Store (CDS).
461 doi: 10.24381/cds.6860a573
462
- 463 Hopcroft, P. O., Kandlbauer, J., Valdes, P. J., & Sparks, R. S. J. (2018). Reduced cooling
464 following future volcanic eruptions. *Climate Dynamics*, 51(4), 1449–1463.
465 <https://doi.org/10.1007/s00382-017-3964-7>
466
- 467 IPCC, 2021: Climate Change 2021: The Physical Science Basis. Contribution of Working
468 Group I to the Sixth Assessment Report of the Intergovernmental Panel on Climate
469 Change [Masson-Delmotte, V., P. Zhai, A. Pirani, S.L. Connors, C. Péan, S. Berger, N.
470 Caud, Y. Chen, L. Goldfarb, M.I. Gomis, M. Huang, K. Leitzell, E. Lonnoy, J.B.R.
471 Matthews, T.K. Maycock, T. Waterfield, O. Yelekçi, R. Yu, and B. Zhou (eds.)].
472 Cambridge University Press, Cambridge, United Kingdom and New York, NY, USA, In
473 press, doi:10.1017/9781009157896.
474
- 475 Kalnay, E., Kanamitsu, M., Kistler, R., Collins, W., Deaven, D., Gandin, L., Iredell, M.,
476 Saha, S., White, G., Woollen, J., Zhu, Y., Chelliah, M., Ebisuzaki, W., Higgins, W.,
477 Janowiak, J., Mo, K. C., Ropelewski, C., Wang, J., Leetmaa, A., Reynolds, R., Jenne, R.,
478 & Joseph, D. (1996). The NCEP/NCAR 40-Year Reanalysis Project, *Bulletin of the*
479 *American Meteorological Society*, 77(3), 437–472. [https://doi.org/10.1175/1520-](https://doi.org/10.1175/1520-0477(1996)077<0437:TNYRP>2.0.CO;2)
480 [0477\(1996\)077<0437:TNYRP>2.0.CO;2](https://doi.org/10.1175/1520-0477(1996)077<0437:TNYRP>2.0.CO;2)
481
- 482 Marshall, L. R., Maters, E. C., Schmidt, A., Timmreck, C., Robock, A., & Toohay, M.
483 (2022). Volcanic effects on climate: recent advances and future avenues. *Bulletin of*
484 *Volcanology*, 84(5), 1–14. <https://doi.org/10.1007/s00445-022-01559-3>
485
- 486 Mastin, L. G. (2007). A user-friendly one-dimensional model for wet volcanic plumes.
487 *Geochemistry, Geophysics, Geosystems*, 8(3). <https://doi.org/10.1029/2006GC001455>
488
- 489 Mastin, L. G. (2014). Testing the accuracy of a 1-D volcanic plume model in estimating
490 mass eruption rate. *Journal of Geophysical Research: Atmospheres*, 119(5), 2474–2495.
491 <https://doi.org/10.1002/2013JD020604>
492
- 493 Mastrandrea, M. D., Field, C. B., Stocker, T. F., Edenhofer, O., Ebi, K. L., Frame, D. J.,
494 Held, H., Kriegler, E., Mach, K. J., Matschoss, P. R., Plattner, G. K. (2010). Guidance
495 note for lead authors of the IPCC fifth assessment report on consistent treatment of
496 uncertainties. <https://>

- 497 www.ipcc.ch/site/assets/uploads/2017/08/AR5_Uncertainty_Guidance_Note.pdf
498
- 499 McCormick, M. P., Thomason, L. W., & Trepte, C. R. (1995). Atmospheric effects of the
500 Mt Pinatubo eruption. *Nature*, 373(6513), 399–404. <https://doi.org/10.1038/373399a0>
501
- 502 Neely III, R.R. & Schmidt, A. (2016). *VolcanEESM: Global volcanic sulphur dioxide*
503 *(SO₂) emissions database from 1850 to present - Version 1.0* [Data set]. Centre for
504 Environmental Data Analysis. [http://dx.doi.org/10.5285/76ebdc0b-0eed-4f70-b89e-](http://dx.doi.org/10.5285/76ebdc0b-0eed-4f70-b89e-55e606bcd568)
505 [55e606bcd568](http://dx.doi.org/10.5285/76ebdc0b-0eed-4f70-b89e-55e606bcd568)
506
- 507 O'Neill, B. C., Tebaldi, C., van Vuuren, D. P., Eyring, V., Friedlingstein, P., Hurtt, G.,
508 Knutti, R., Kriegler, E., Lamarque, J.-F., Lowe, J., Meehl, G. A., Moss, R., Riahi, K., &
509 Sanderson, B. M. (2016). The Scenario Model Intercomparison Project (ScenarioMIP)
510 for CMIP6. *Geoscientific Model Development*, 9(9), 3461–3482.
511 <https://doi.org/10.5194/gmd-9-3461-2016>
512
- 513 Pausata, F. S. R., Chafik, L., Caballero, R., & Battisti, D. S. (2015). Impacts of high-
514 latitude volcanic eruptions on ENSO and AMOC. *Proceedings of the National Academy*
515 *of Sciences*, 112(45), 13784–13788. <https://doi.org/10.1073/pnas.1509153112>
516
- 517 Santer, B. D., Bonfils, C., Painter, J. F., Zelinka, M. D., Mears, C., Solomon, S., Schmidt,
518 G. A., Fyfe, J. C., Cole, J. N. S., Nazarenko, L., Taylor, K. E., & Wentz, F. J. (2014).
519 Volcanic contribution to decadal changes in tropospheric temperature. *Nature*
520 *Geoscience*, 7(3), 185–189. <https://doi.org/10.1038/ngeo2098>
521
- 522 Schmidt, A., Mills, M. J., Ghan, S., Gregory, J. M., Allan, R. P., Andrews, T., Bardeen,
523 C. G., Conley, A., Forster, P. M., Gettelman, A., Portmann, R. W., Solomon, S., & Toon,
524 O. B. (2018). Volcanic Radiative Forcing From 1979 to 2015. *Journal of Geophysical*
525 *Research: Atmospheres*, 123(22), 12491–12508. <https://doi.org/10.1029/2018JD028776>
526
- 527 Mulcahy, J. P., Jones, C. G., Rumbold, S. T., Kuhlbrodt, T., Dittus, A. J., Blockley, E.
528 W., Yool, A., Walton, J., Hardacre, C., Andrews, T., Bodas-Salcedo, A., Stringer, M., de
529 Mora, L., Harris, P., Hill, R., Kelley, D., Robertson, E., & Tang, Y. (2023). UKESM1.1:
530 Development and evaluation of an updated configuration of the UK Earth System Model.
531 *Geoscientific Model Development Discussions*, in press. [https://doi.org/10.5194/gmd-](https://doi.org/10.5194/gmd-2022-113)
532 [2022-113](https://doi.org/10.5194/gmd-2022-113)
533
- 534 Sigl, M., Toohey, M., McConnell, J. R., Cole-Dai, J., & Severi, M. (2022). Volcanic
535 stratospheric sulfur injections and aerosol optical depth during the Holocene (past 11 500
536 years) from a bipolar ice-core array. *Earth System Science Data*, 14(7), 3167–3196.
537 <https://doi.org/10.5194/essd-14-3167-2022>
538
- 539 Sigl, M., Winstrup, M., McConnell, J. R., Welten, K. C., Plunkett, G., Ludlow, F.,
540 Büntgen, U., Caffee, M., Chellman, N., Dahl-Jensen, D., Fischer, H., Kipfstuhl, S.,
541 Kostick, C., Maselli, O. J., Mekhaldi, F., Mulvaney, R., Muscheler, R., Pasteris, D. R.,
542 Pilcher, J. R., ... Woodruff, T. E. (2015). Timing and climate forcing of volcanic

543 eruptions for the past 2,500 years. *Nature*, 523(7562), 543–549.
544 <https://doi.org/10.1038/nature14565>

545
546 Stoffel, M., Khodri, M., Corona, C., Guillet, S., Poulain, V., Bekki, S., Guiot, J.,
547 Luckman, B. H., Oppenheimer, C., Lebas, N., Beniston, M., & Masson-Delmotte, V.
548 (2015). Estimates of volcanic-induced cooling in the Northern Hemisphere over the past
549 1,500 years. *Nature Geoscience*, 8(10). <https://doi.org/10.1038/ngeo2526>

550
551 Timmreck, C., Mann, G. W., Aquila, V., Hommel, R., Lee, L. A., Schmidt, A., Brühl, C.,
552 Carn, S., Chin, M., Dhomse, S. S., Diehl, T., English, J. M., Mills, M. J., Neely, R.,
553 Sheng, J., Toohey, M., & Weisenstein, D. (2018). The Interactive Stratospheric Aerosol
554 Model Intercomparison Project (ISA-MIP): Motivation and experimental design.
555 *Geoscientific Model Development*, 11(7), 2581–2608. [https://doi.org/10.5194/gmd-11-](https://doi.org/10.5194/gmd-11-2581-2018)
556 2581-2018

557
558 Zambri, B., Robock, A., Mills, M. J., & Schmidt, A. (2019). Modeling the 1783–1784
559 Laki Eruption in Iceland: 2. Climate Impacts. *Journal of Geophysical Research:*
560 *Atmospheres*, 124(13), 6770–6790. <https://doi.org/10.1029/2018JD029554>